U.S. DEPARTMENT OF COMMERCE
NATIONAL OCEANIC AND ATMOSPHERIC ADMINISTRATION
NATIONAL WEATHER SERVICE
NATIONAL METEOROLOGICAL CENTER

OFFICE NOTE 384

A NOTE ON THE DIVERGENCE DAMPER AS A MEANS OF NOISE CONTROL IN A NUMERICAL HURRICANE PREDICTION MODEL

ALAN SHAPIRO
UCAR VISITING POST-DOCTORAL SCIENTIST

NOVEMBER 1991

A Note on the Divergence Damper as a Means of Noise Control in a Numerical Hurricane Prediction Model

by Alan Shapiro, UCAR visiting postdoctoral scientist

I. Introduction

One of the ongoing challenges in numerical weather prediction is the reduction of spurious inertio-gravity wave noise in numerical prediction models. This noise, if left unchecked, can seriously degrade the quality of a forecast. Acceptable methods of noise control reduce the amplitude of these waves without contaminating the meteorologically relevant scales of motion. The adequacy of a procedure is thus partially dependent on the nature of the atmospheric flows a model is designed to represent.

This note investigates the use of a "divergence damper" as a means of noise control in the National Meteorological Center's (NMC) operational hurricane prediction model, the Quasi-Lagrangian Model (QLM). The damper appears explicitly in the model as an extra term in the equations of motion,

$$\frac{\partial \vec{V}}{\partial t} = \ldots + \kappa \nabla D, \qquad D \equiv \nabla_H \cdot \vec{V} \tag{1}$$

Here κ is the damping term's constant damping coefficient. The corresponding divergence equation,

$$\frac{\partial D}{\partial t} = \ldots + \kappa \nabla^2 D \tag{2}$$

shows that the damper dissipates noise by diffusing divergence.

The impact of the divergence damper is investigated first with a simple theoretical model (section II) and then with a series of experiments performed in the QLM (section III). A discussion of these results and recommendations for the use of the damper follow in section IV.

II. Theoretical considerations

As a crude check on the possible impact of the damper on a forecast, we derive a characteristic time scale for the divergence damping of a divergent secondary circulation. We consider the simple initial value problem for an axisymmetric secondary circulation with divergence damping as the only forcing:

$$\frac{\partial u}{\partial t} = \kappa \frac{\partial D}{\partial r} \qquad \text{where} \qquad D = \frac{1}{r}\frac{\partial ru}{\partial r} \tag{3}$$

Here u is the radial wind component, r the cylindrical polar radius and t is the time.

Seeking solutions of the form:

$$u(t, r) = f(t)\, g(r) \tag{4}$$

leads to a set of ordinary differential equations involving a separation constant λ:

$$\frac{f'(t)}{f} = \kappa\left(\frac{g''(r)}{g} + \frac{g'(r)}{rg} - \frac{1}{r^2}\right) = -\lambda \tag{5}$$

Solving (5) subject to the condition that the axis of symmetry not be a source or sink of mass, i.e., u(t,0) = 0, yields:

$$u(t, r) = A\, e^{-\lambda t}\, J_1\left(\sqrt{\frac{\lambda}{\kappa}}\, r\right) \tag{6}$$

where J_1 is the Bessel function of the first kind of order 1 and A is an arbitrary constant. From (6) we can clearly identify λ as the reciprocal e-folding time scale for the divergence damper.

We now introduce an outer radius R which defines the scale of the secondary circulation, viz, $u(t, R) \equiv 0$. Making use of (6) and the definition of R, we can establish a relation between the time scale parameter, λ, and both the divergence damping coefficient, κ, and the outer radius of the inflow circulation, R. Since the first zero of

the Bessel function $J_1(x)$ occurs at x = 3.83 (Jahnke and Emde, 1945) this relation may be written as:

$$\lambda = \kappa\left(\frac{3.83}{R}\right)^2 \tag{7}$$

The spatial part of u(t, r), the inflow circulation on which we are imposing the divergence damper, is graphed in Fig. 1.

In the QLM the damping constant is given by $\kappa = 2$ XKD Δ where Δ = 40,000 m is the model grid spacing and XKD is a numerical coefficient assigned an operational value of 30. With these values the characteristic e-folding time scale $\tau \equiv 1/\lambda$ is given by:

$$\tau = 0.0284\ R^2\ (s^{-1}) \tag{8}$$

with R expressed in kilometers. Examples of τ 's quadratic dependence on R based on formula (8) is presented in Table 1. The damping time scale is seen to increase from just under a minute for small scale disturbances of the size of the QLM grid spacing (R = 40 km) to over a week for large scale synoptic disturbances (R = 5000 km).

Although the derivation of (8) for the damping time scale, τ, was rather simplistic, the results may have a qualitative significance and deserve some mention. We offer them here as hypotheses to be checked against the results of the QLM experiments described in the next section:

(i) noise on a horizontal scale of the QLM grid spacing (40 km) can be effectively reduced by the divergence damper.

(ii) For 0 - 72 hour forecasts the large scale synoptic flow should be relatively unaffected by the damper.

(iii) For 0 - 72 hour forecasts the divergent circulation of some hurricane scale disturbances (R < 1000 km) may be significantly attenuated by the damper.

III. Numerical experiments with the divergence damper

As a test of hypotheses (i) - (iii) of section II, numerical experiments with the divergence damper were performed in a high resolution hurricane prediction model, the NMC's QLM. The operational version of this model solves the primitive equations over a 4400 km^2 square domain with a 40 km horizontal grid spacing and 16 σ-levels in the vertical. A one-step second order quasi-Lagrangian scheme (Mathur, 1983) performs the time integrations. Because of analysis difficulties, a bogus vortex is applied directly on the model grid as part of the initialization procedure. In the operational version of the model a dipole perturbation wind field is then superimposed on the bogus vortex to serve, in part, as a steering current. We have omitted this latter stage of the initialization from our experiments since it is not fundamental to the problem at hand, i.e. understanding the workings of the divergence damper, and may add undue complexity to the results. Details of the QLM, including model structure, physical parameterizations, boundary conditions and initialization procedures can be found in Mathur (1991).

A sample of four storms were considered in these experiments: Fabio on 12Z 2 August 1988, Gilbert on 12Z 10 September 1988, when it was relatively weak, Gilbert again on 12Z 14 September 1988 when it was billed as the "storm of the century" and Hugo on 00Z 21 September 1989. Model integrations were carried out over a 0-72 hour forecast period first with the divergence damper fixed at the operational value of XKD = 30 and then with successively lower values of XKD.

In all experiments a storm-dependent lower bound of XKD was obtained beyond which the model became unstable. We refer to the value of this lower bound as the "critical XKD" value. It was found that forecasts of Fabio, Gilbert (10 Sept), Gilbert (14 Sept) and Hugo were stable throughout the 0-72 hour forecast period at XKD values of 3, 5, 15, and 10 respectively, but unstable at values of 1, 3, 10 and 5. The critical XKD values for these storms thus lie in the ranges 1-3, 3-5, 10-15 and 5-10. It can be noted from Tables 2-5 that the two strongest storms (i.e. having the lowest central pressure), Gilbert on 14 Sept. and Hugo, had critical XKD values at least twice as large as the two weakest storms, Gilbert on 10 Sept. and Fabio.

We now turn our attention to the impact of the damper on the hurricane circulation. Time series of the predicted rainfall intensity and central sea level pressure are provided in Tables 2-5 for each of the four storms with the original operational XKD value of 30 and with the lowest value of XKD which resulted in a stable 0-72 hour forecast. In all cases a reduced divergence damper resulted in a significant increase in the peak predicted rainfall intensity (12 hour accumulated rainfall). For many 12 hour periods the increase amounted to 2-3 inches. The average increases were approximately 10% for Hugo (XKD=10), 15% for Gilbert on Sept 14 (XKD=15), 50% for Gilbert on Sept 10 (XKD=5) and 80% for Fabio (XKD=3). It can be noted that the storms with the lowest XKD values (Fabio and Gilbert on Sept 10) were impacted the most. During at least three separate 12 hour forecast periods the peak rainfall rates for these latter two storms were more than doubled by the reduced damper. Unfortunately it was not possible to verify any of these rainfall predictions due to a lack of observations.

Despite the significant change in rainfall rates there was only a slight change in the evolution of the central sea level pressure with a reduced damper. The most striking feature, a jump in the predicted central pressure within the first 6 hours (which did not verify against observations as reported in the National Weather Service's hurricane advisories), was apparent in all experiments, regardless of XKD value. In the experiments with the two lowest values of XKD (Fabio and Gilbert on Sept 10), there was a slight decrease in the time averaged PC, of the order of 1 mb, compared to the PC in the corresponding XKD=30 experiments. The time averaged PC for Gilbert on Sept 14 remained essentially unchanged while the time averaged PC for Hugo rose by a fraction of a millibar.

The reduced damping procedure left relatively unchanged not only the storm central pressure but also pressure features on the synoptic scale. As representative examples, consider the predicted surface pressure field 6 hours into the Fabio forecast (Fig. 2) with (a) XKD =30 and (b) XKD = 3 and 36 hours into the Gilbert (Sept 14) forecast (Fig. 3) with (a) XKD = 30 and (b) XKD = 15. The location and amplitude of the highs, lows, ridges, troughs, etc is hardly affected by the reduced damping.

A revealing comparison can be made of the operational and reduced damper predictions for the 1000 mb wind field. In nearly every forecast period the peak wind speeds in a reduced damper

storm were increased significantly over those in the corresponding operationally damped storm. In many cases the peak wind speeds were nearly doubled. Furthermore, the orientation of the velocity vectors reveals that a significant portion of this wind increase was due to an increased radial inflow, i.e., an increase in the divergent wind component. Representative examples of the 1000 mb wind forecasts given in Figs. 4 and 5 are for the same experiments considered in Figs. 2 and 3. Fabio's 6 hour predicted peak wind of 19 m/s for the operational damping of XKD=30 compares with a 33 m/s maximum for a reduced damping of XKD=3. Similarly, Gilbert's (14 Sept) 36 hour predicted peak wind rose from 33 m/s for XKD=30 to 51 m/s for a reduced damping of XKD=15. This latter wind speed, valid at 0000Z Sept. 16, is quite close to the 120 mph (55 m/s) reported in the National Weather Service's intermediate advisory issued at 8 pm CDT Sept. 15 (0100Z Sept. 16). However, despite the good agreement, one should keep in mind that this observed peak wind speed almost certainly occurs at a pressure less than 1000 mb whereas the comparison is made with predicted 1000 mb winds.

The damper's dramatic effect on the 1000 mb wind field was, however, confined to the inner region of the vortex, just a few grid points from the storm center; beyond this inner region there were relatively minor differences. Despite Fabio's increase in peak wind strength (Fig. 4), the area enclosed by the 10 m/s isotach was increased only slightly by the reduced damping. Similarly, for Gilbert (Fig. 5), the areas enclosed by the 10, 20 and 30 m/s isotachs were hardly affected by the reduced damping. (Note: the velocity vector scalings in Figs. 4 and 5 depend upon the peak wind speed.)

Finally, it can be noted that the predicted storm tracks (not shown) were relatively insensitive to the amount of divergence damping. Typical track discrepancies were on the order of 1-2 grid points with no discernible directional or speed preferences.

IV. Discussion

The numerical experiments described in section III were performed to corroborate/refute the hypotheses advanced in section II on the impact of the divergence damper on a numerical hurricane prediction model. These hypotheses will now be examined in light of these experiments.

We consider first the results on model stability. For each of the four storms considered in this investigation, a storm-dependent lower bound of the damping coefficient XKD was obtained beyond which the model became unstable. As a corollary, there was a storm-dependent upper bound of XKD beyond which the model became stable. The finding that the weak storms had lower critical XKD values than the strong storms is not unexpected as stronger storms may generate more noise in the initialization procedure and in their subsequent interaction with model boundaries and thus require more damping. In any event, the fact that the model became stable for large enough XKD values is testimony to the effectiveness of the divergence damper as a means of noise control, in accord with hypothesis (i).

The relative insensitivity of the large scale wind and pressure fields to a reduction in the damper (as depicted, for example, in Figs. 2-5) supports the validity of hypothesis (ii). It appears that the divergence damper with XKD coefficient set to an operational value of 30 does not adversely affect features on the synoptic scale.

On the other hand, the increase in peak rainfall rate with damper reduction, or, perhaps of more relevance, the decrease in rainfall rate with damper increase (Tables 2-5) points to a potentially undesirable side effect of the damper as a means of noise control. The increased rainfall was found in association with a dramatic intensification of the winds in the inner region of the vortex, an increase supported to a large extent by a strengthened radial inflow (Figs. 4 and 5). Presumably it was this increased radial inflow which sustained the increased rainfall rate in the storm center. The damper's impact on the hurricane's divergent secondary circulation as anticipated by hypothesis (iii) is consistent with these results.

The finding that the increased rainfall rate and peak wind speeds are unaccompanied by a significant decrease in central pressure would, at first, appear rather mysterious. Intuitively one would expect a substantial lowering of the central pressure to support an increased centripetal acceleration in the vortex core. In the present instance, however, the wind increase may be due largely to an increased radial inflow without a substantially changed tangential wind (which is at least suggested by Figs. 4 and 5). The confinement of a noticable peak wind increase to a narrow region encircling the storm center is entirely consistent with a picture of an increased boundary layer mass influx converging and erupting upwards at the

storm center. Assuming this to be the case, it is instructive to isolate the role of the secondary circulation in the pressure balance by integrating an (axisymmetric) radial equation of motion,

$$\ldots + u_r \frac{\partial u_r}{\partial r} + \ldots = -\frac{1}{\rho}\frac{\partial p}{\partial r} + \ldots \quad \text{to obtain} \quad p(r) = p(R) - \frac{u_r^2(r)}{2} + \ldots$$

i.e., a quadratic dependence of the pressure drop on the radial (divergent) wind component. Since the radial wind must vanish at the storm center to satisfy mass conservation, the pressure drop due to the radial wind component is always nullified at the storm center regardless of the radial wind distribution leading up to the storm center. This effect is in marked distinction to the integral effect of the centripetal acceleration. Thus, in view of the predicted wind and pressure distributions typified by Figs. 2-5 and the above considerations, it seems likely that the changes in the peak wind speed were dominated by changes in the radial (divergent) wind.

It can be noted that other experiments on the divergence damper have been previously undertaken at the NMC (cited by Haltiner and Williams, 1980). The damper's ability to suppress noise in an 8-layer σ-coordinate primitive equation model was also found to affect meteorologically relevant flows. Of particular significance was the generation of high pressure anomalies in the vicinity of mountains and the elimination of precipitation for sufficiently high damping coefficients.

In summary, a simple theoretical analysis supported by numerical experimentation in the QLM suggest that the divergence damper can effectively control noise but at a cost to a divergent hurricane secondary circulation. The problem may stem from the damper's inability to distinguish between divergent gravity wave noise and divergent in-up-out secondary circulations typical of hurricanes. Curiously, the damper's reduction of storm intensity as evidenced by a decreased peak rainfall intensity and inner core wind strength had little effect on the storm track. It would thus appear that the use of the damper is justified in a model designed primarily for storm track prediction rather than for hurricane intensity prediction.

References

Jahnke, E. and Emde, F., 1945: *Tables of Functions.* Dover Publications.

Haltiner, G. J. and Williams, R. T., 1980: *Numerical Prediction and Dynamic Meteorology* (second edition). John Wiley and Sons, Inc., 477 pp.

Mathur, M. B., 1983: A quasi-Lagrangian regional model designed for operational weather prediction. *Mon. Wea. Rev.*, **111**, 2087-2098.

Mathur, M. B., 1991: The National Meteorological Center's Quasi-Lagrangian Model for Hurricane Prediction. *Mon. Wea. Rev.*, **119**, 1419-1447.

R (km)	τ
40	45.4 sec
100	4.7 min
200	18.9 "
300	42.6 "
400	1.3 hr
500	2.0 "
600	2.8 "
700	3.9 "
800	5.0 "
900	6.4 "
1000	7.9 hr
2000	1.3 day
3000	3.0 "
4000	5.3 "
5000	8.2 "

Table 1. The e-folding divergence damping time scale, τ, as a function of the radius, R, of an imposed secondary circulation. The damping coefficient is specified according to the QLM prescription, viz $\kappa = 2 \cdot 30 \cdot 40{,}000$.

Fabio 12 Z 2 Aug 1988

	XKD = 30		XKD = 3	
time	PC	rain	PC	rain
0	976		976	
6	998	1.8	997	2.8
12	1000	3.8	998	7.1
24	1001	2.0	1001	2.9
36	1003	1.7	1004	1.9
48	1004	1.5	1005	2.7
60	1005	0.87	1005	1.9
72	1006	0.61	1005	2.1
average:	999.1	1.7	998.9	3.1

Table 2: QLM forecast central pressure, PC (mbs), and peak rainfall intensity (inches/12 hrs except for t =0-6 hrs) for Fabio 12 Z 2 Aug 1988 as a function of divergence damping coefficient, XKD. An initial PC value of 980 was applied in the vortex bogussing procedure.

Gilbert 12Z 10 Sept 1988

	XKD = 30		XKD = 5	
time	PC	rain	PC	rain
0	999		999	
6	1003	0.97	1002	1.9
12	1001	2.2	999	5.8
24	998	3.7	1000	2.9
36	996	2.0	997	4.2
48	998	2.3	995	4.1
60	997	3.0	993	6.9
72	1004	0.94	998	5.6
average:	999.5	2.4	997.9	4.9

Table 3: QLM forecast central pressure, PC (mbs), and peak rainfall intensity (inches/12 hrs except for t =0-6 hrs) for Gilbert 12Z 10 Sept 1988 as a function of divergence damping coefficient, XKD. An initial PC value of 1000 mb was applied in the vortex bogussing procedure.

Gilbert 12Z 14 Sept. 1988

	XKD = 30		XKD = 15	
time	PC	rain	PC	rain
0	964		964	
6	977	2.8	977	3.8
12	980	5.9	979	7.1
24	977	6.0	976	6.3
36	973	8.9	972	11
48	971	8.5	973	11
60	979	8.6	979	10
72	990	5.4	991	4.5
average:	976.4	7.2	976.4	8.3

Table 4: QLM forecast central pressure, PC (mbs), and peak rainfall intensity (inches/12 hrs except for t =0-6 hrs) for Gilbert 12Z 14 Sept. 1988 as a function of divergence damping coefficient, XKD. An initial PC value of 970 mb was applied operationally in the vortex bogussing procedure (and in this experiment) although the observed value was 890 mb.

Hugo 00Z 21 Sept 1989

	XKD = 30		XKD = 10	
time	PC	rain	PC	rain
0	944		944	
6	981	4.2	980	5.0
12	983	7.6	984	10.
24	986	3.5	991	2.3
36	992	3.3	995	3.0
48	994	2.1	995	2.6
60	986	1.7	985	2.4
72	992	0.82	994	0.51
average:	982.3	3.2	983.5	3.5

Table 5: QLM forecast central pressure, PC (mbs), and peak rainfall intensity (inches/12 hrs except for t =0-6 hrs) for Hugo 00Z 21 Sept 1989 as a function of divergence damping coefficient, XKD. An initial PC value of 950 mb was used in the vortex bogussing procedure.

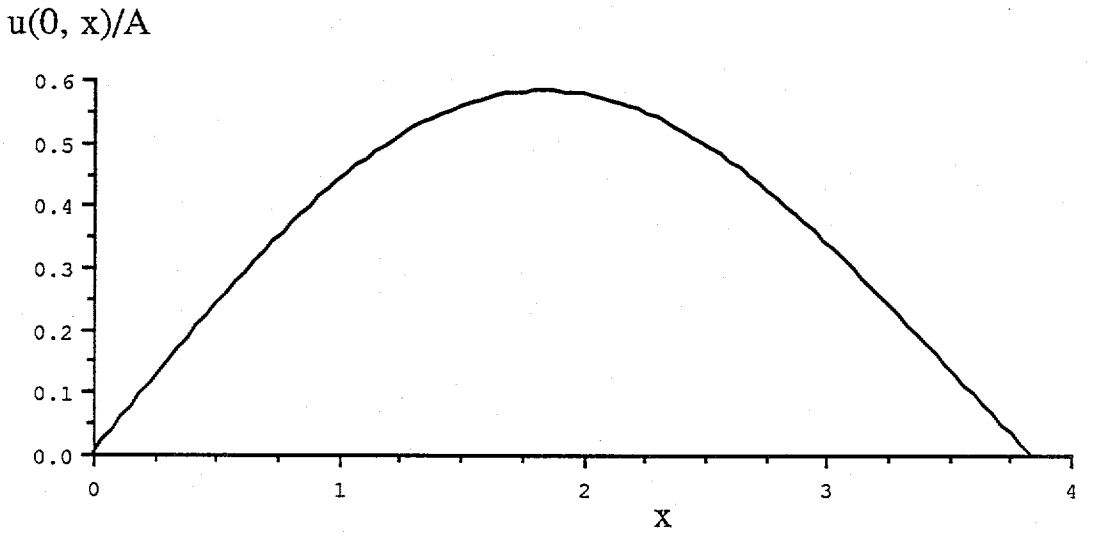

Fig. 1. Radial dependence of the inflow velocity used to estimate the divergence damper time scale. The non-dimensional radial coordinate $x \equiv (\lambda/\kappa)^{1/2} r$ is the argument of $J_1(x)$.

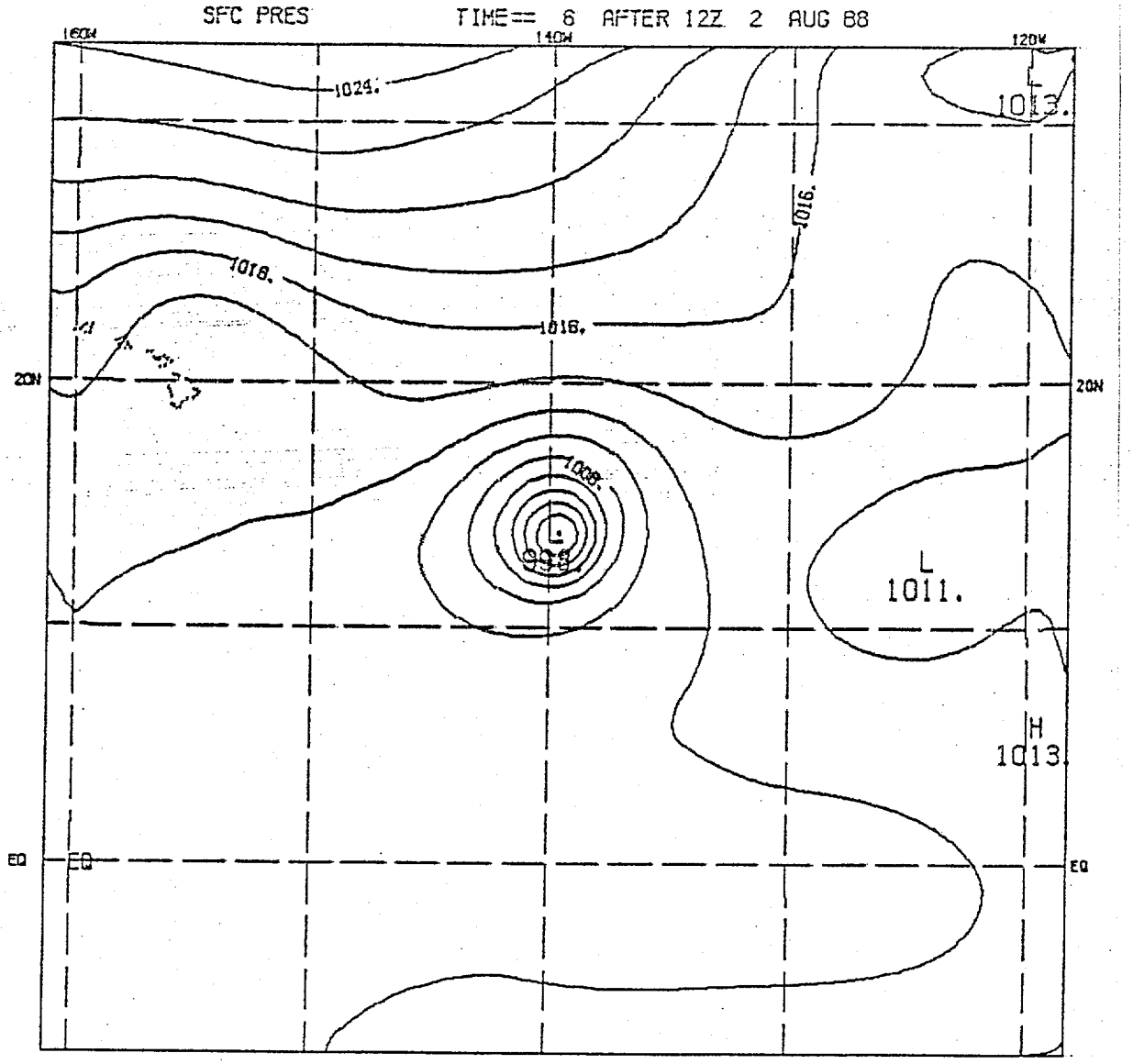

Fig. 2. (a) XKD = 30. 6 hour forecast of surface pressure field for Fabio.

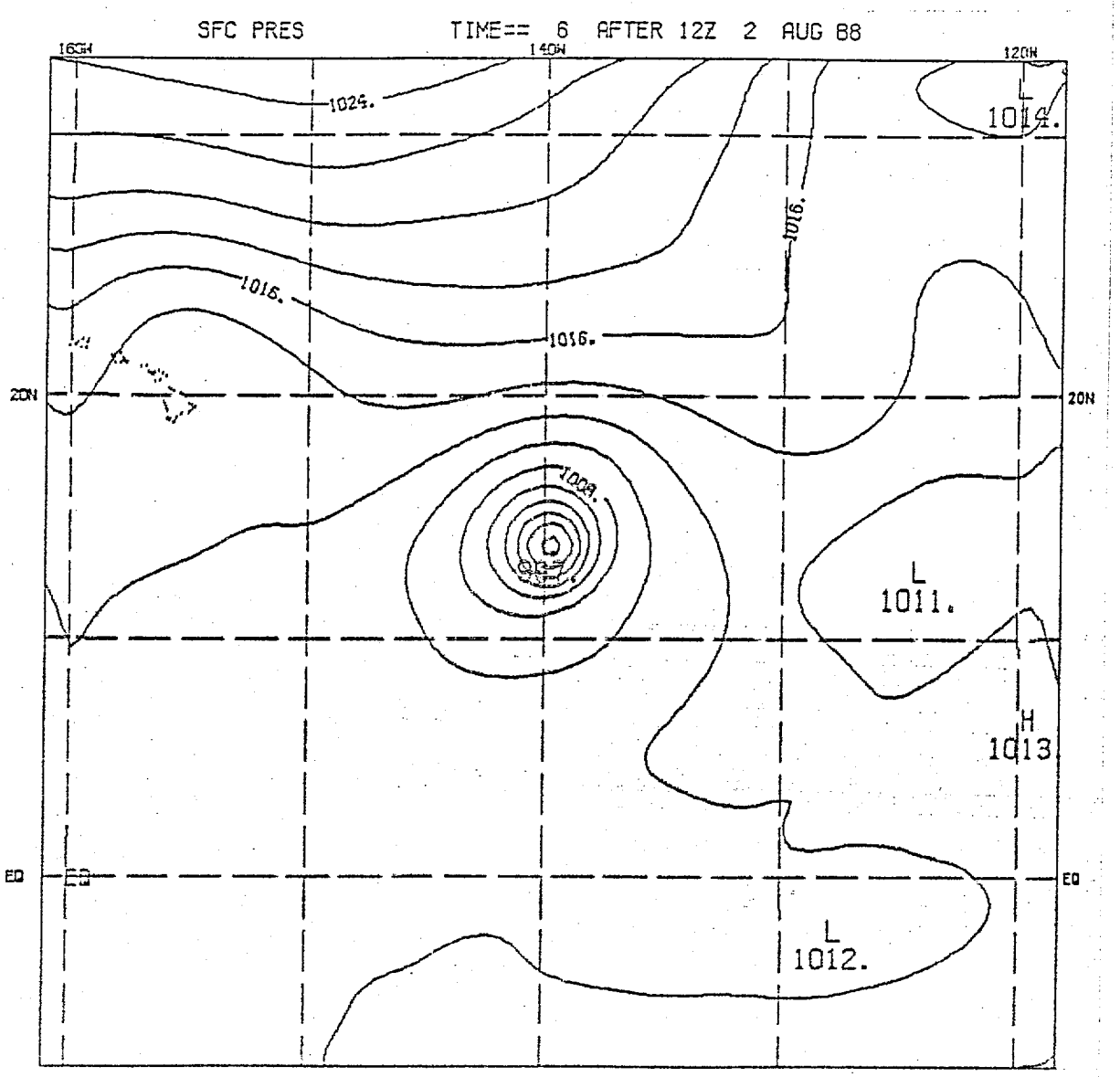

Fig. 2. (b) XKD = 3. 6 hour forecast of surface pressure field for Fabio.

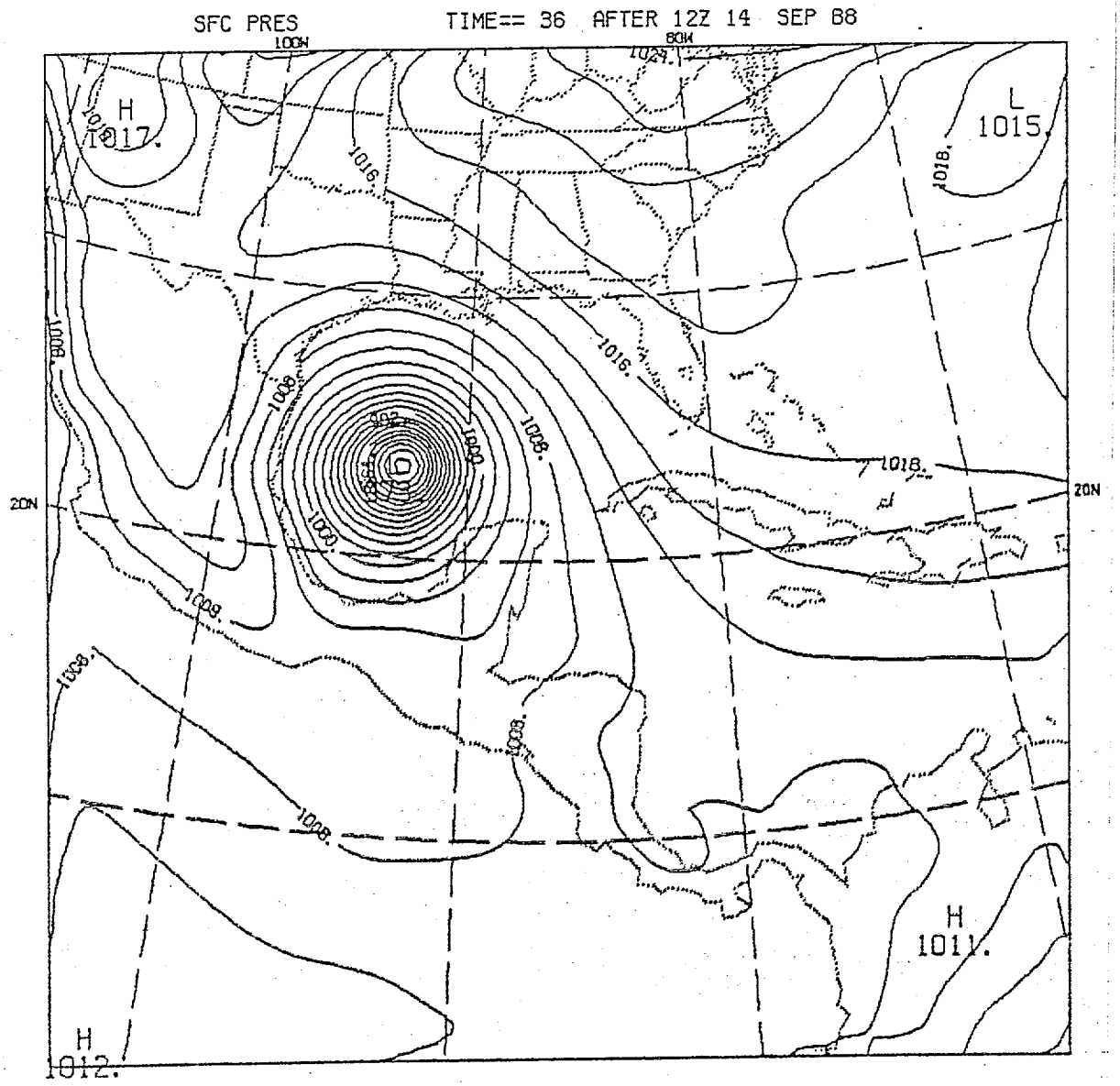

Fig. 3. (a) XKD = 30. 36 hour forecast of surface pressure field for Gilbert (14 Sept).

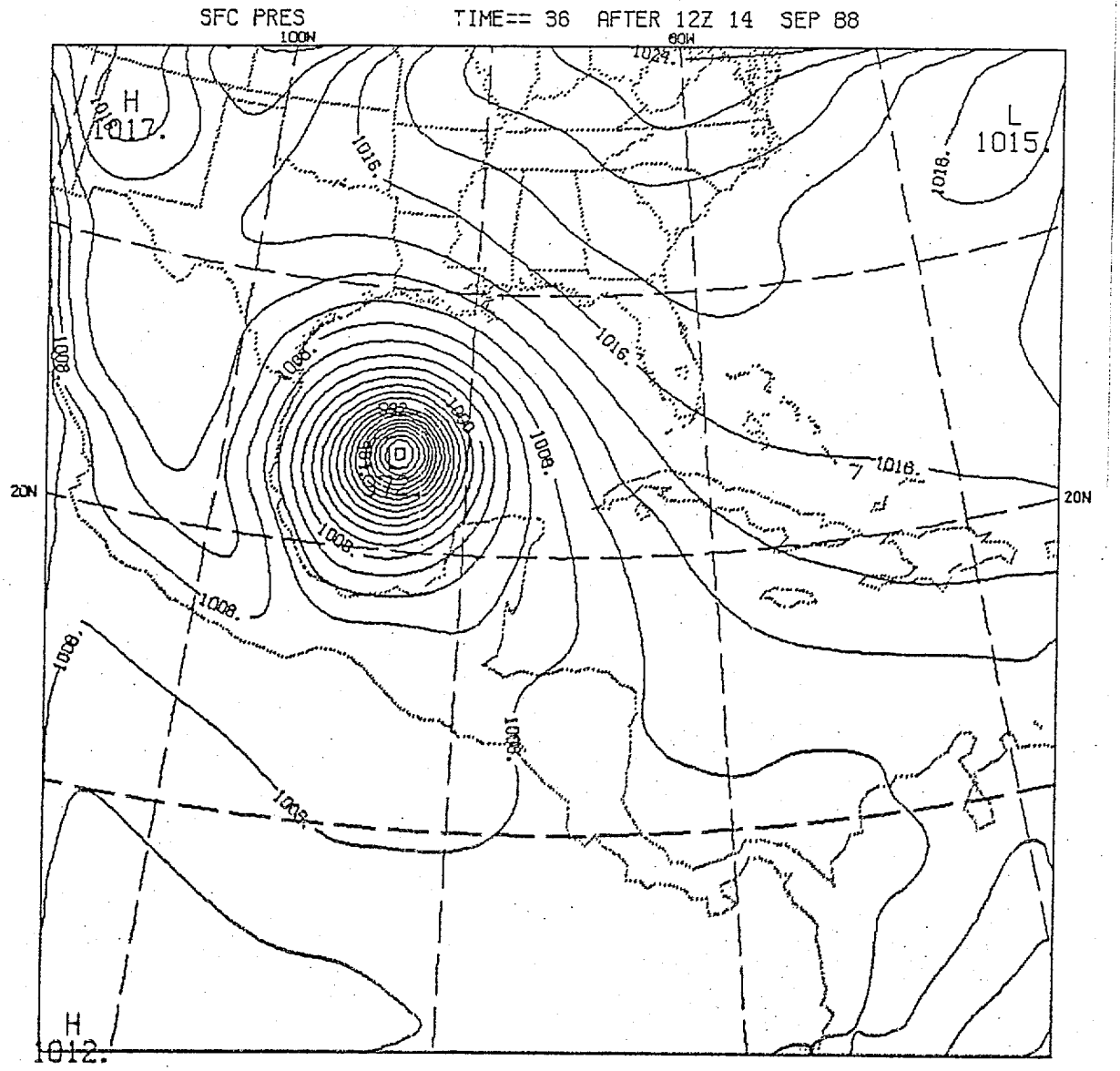

Fig. 3. (b) XKD = 15. 36 hour forecast of surface pressure field for Gilbert (14 Sept).

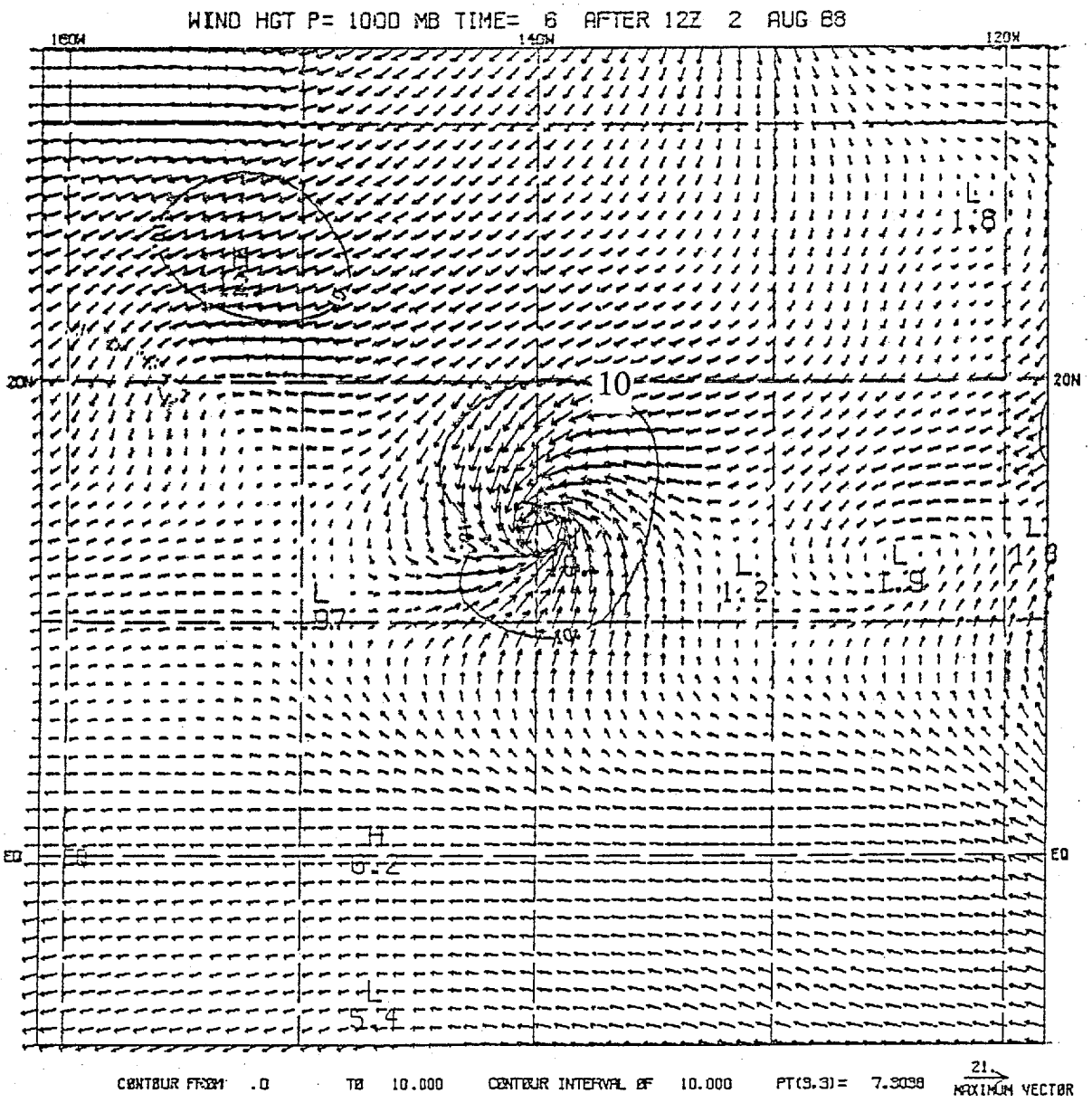

Fig. 4. (a) XKD = 30. 6 hour forecast of 1000 mb wind field for Fabio. Note: owing to differences in maximum wind speeds, wind vectors in (a) and (b) are scaled differently. Maximum wind speed in (a) is 19 m/s.

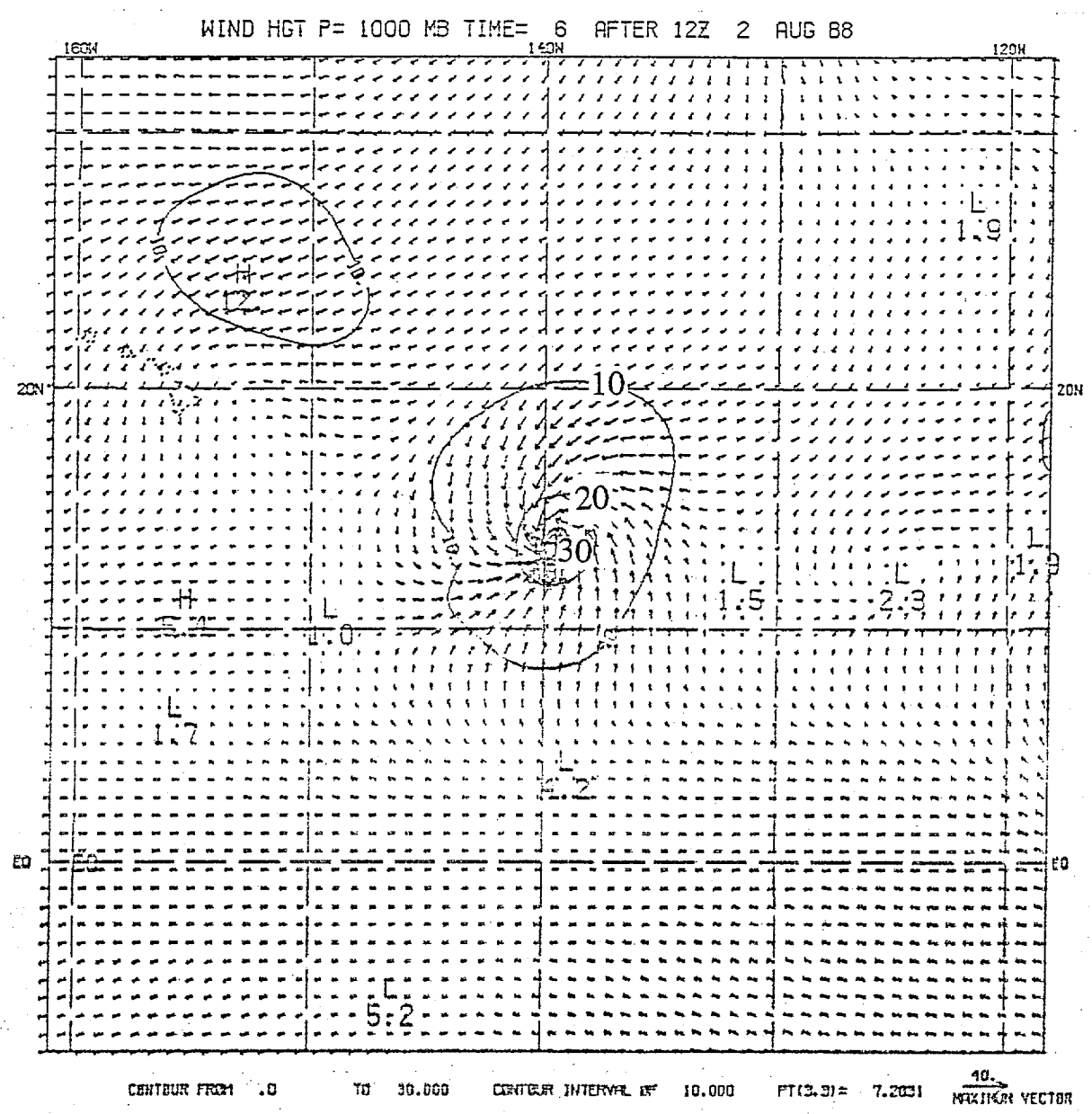

Fig. 4. (b) XKD = 3. 6 hour forecast of 1000 mb wind field for Fabio. Note: owing to differences in maximum wind speeds, wind vectors in (a) and (b) are scaled differently. Maximum wind speed in (b) is 33 m/s.

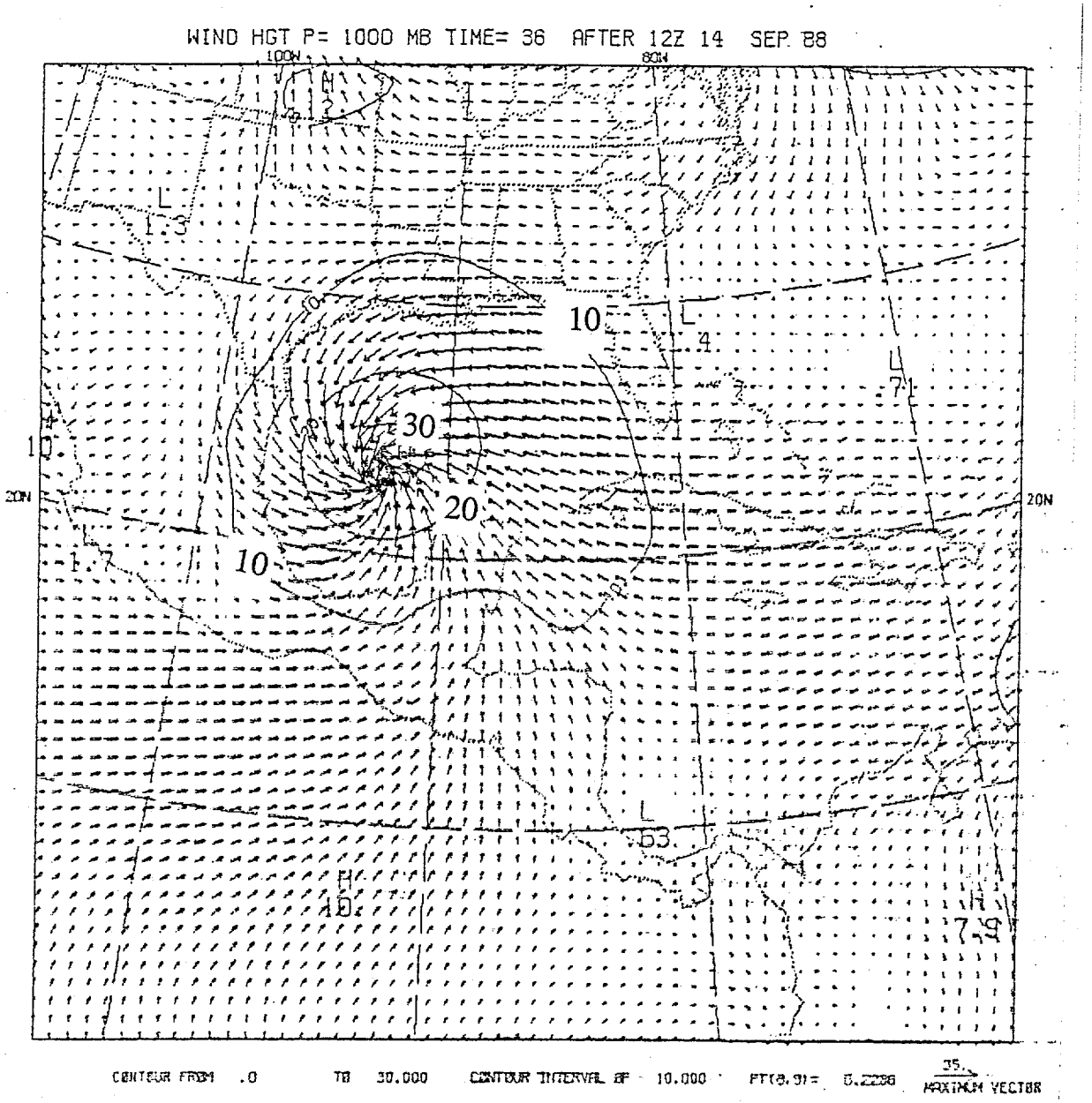

Fig. 5. (a) XKD = 30. 36 hour forecast of 1000 mb wind field for Gilbert (14 Sept). Note: owing to differences in maximum wind speeds, wind vectors in (a) and (b) are scaled differently. Maximum wind speed in (a) is 33 m/s.

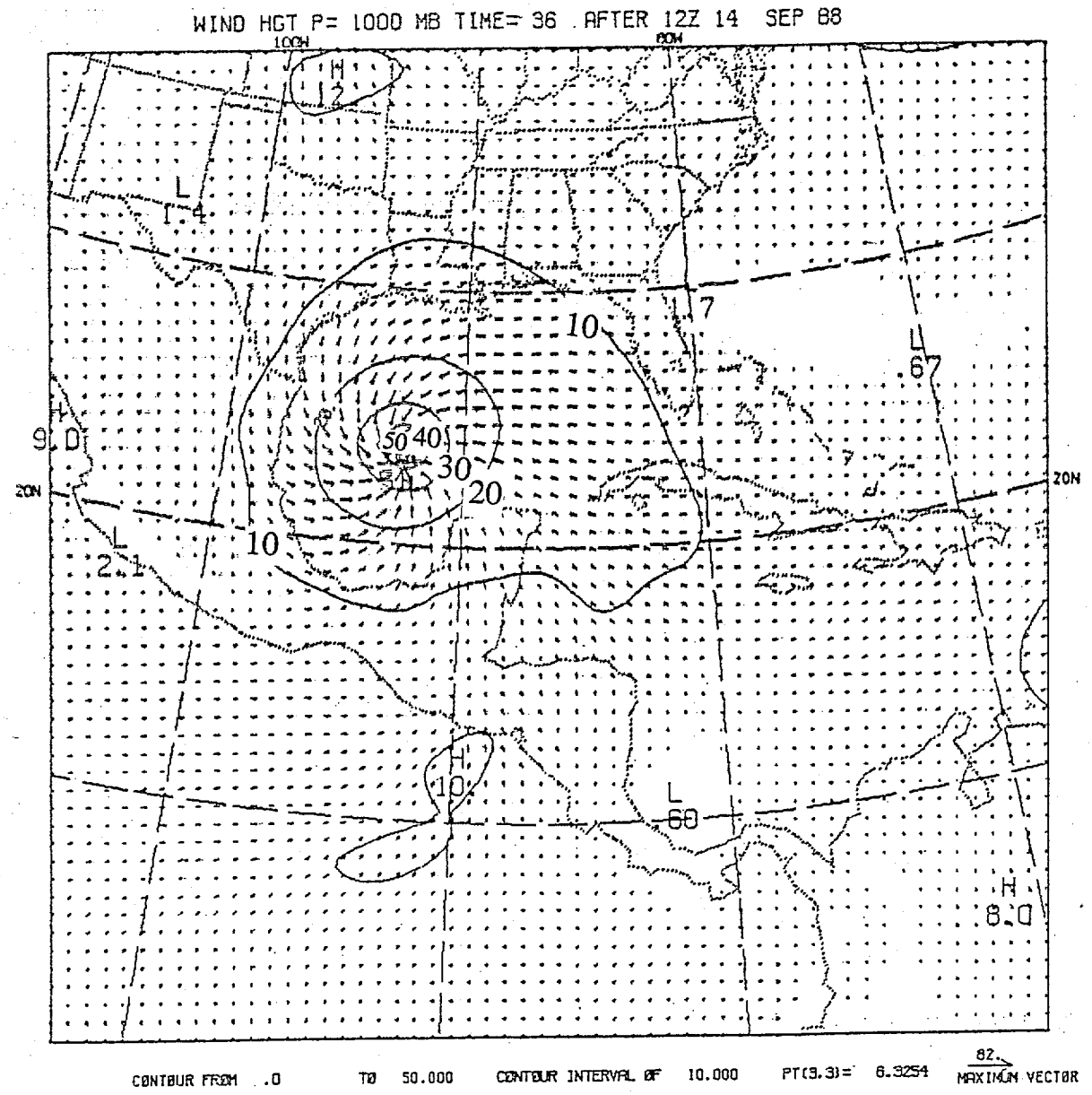

Fig. 5. (b) XKD = 15. 36 hour forecast of 1000 mb wind field for Gilbert (14 Sept). Note: owing to differences in maximum wind speeds, wind vectors in (a) and (b) are scaled differently. Maximum wind speed in (b) is 51 m/s.